machines

MDPI

Article

Efficient Surrogate-Assisted Parameter Analysis for Coal-Supercritical Water Fluidized Bed Reactor with Adaptive Sampling

Pu Zhao, Haitao Liu *, Xinyu Xie, Shiqi Wang, Jiali Liu, Xiaofang Wang, Rong Xie and Siyuan Zuo

School of Energy and Power Engineering, Dalian University of Technology, Dalian 116024, China
* Correspondence: htliu@dlut.edu.cn

Abstract: Supercritical water fluidized beds (SCWFBs) are promising and efficient reactors for the gasification of coal in supercritical water. The understanding and investigation of multi-phase flows as well as the gasification process usually rely on time-consuming experiments or numerical simulations, which prohibit fast and full exploration of the single and coupled effects of the operation and geometric parameters. To this end, this paper builds an efficient surrogate-assisted parameter analysis framework for the SCWFB reactor. Particularly, (1) it establishes a steady numerical simulation model of the SCWFB reactor for the subsequent analysis; and (2) it employs a Gaussian process surrogate modeling via efficient adaptive sampling to serve as an approximation for predicting the carbon conversion efficiency (CE) of the reactor. Based on this parameter analysis framework, this paper investigates the effects of five independent parameters (the mass flow rate of supercritical water, mass flow rate of the coal slurry, temperature of supercritical water, temperature of the outer wall and reactor length) and their interactions on the reaction performance in terms of the carbon conversion efficiency (CE). We found that the CE increases as a function of the temperature of supercritical water, the temperature of the outer wall and the reactor length; while it decreases as a function of the mass flow rate of supercritical water and the mass flow rate of the coal slurry. Additionally, the global sensitivity analysis demonstrates that the influence of the temperature of the outer wall exerts a stronger effect than all the other factors on the CE, and the coupled interaction among parameters has a slight effect on the CE. This research provides useful guidance for scaled-up designs and optimization of the SCWFB reactor.

Keywords: supercritical water gasification; fluidized bed; Gaussian process; adaptive sampling; parametric analysis

Citation: Zhao, P.; Liu, H.; Xie, X.; Wang, S.; Liu, J.; Wang, X.; Xie, R.; Zuo, S. Efficient Surrogate-Assisted Parameter Analysis for Coal-Supercritical Water Fluidized Bed Reactor with Adaptive Sampling. *Machines* **2023**, *11*, 295. https://doi.org/10.3390/machines11020295

Academic Editors: Imre Ferenc Barna and Krisztian Hriczo

Received: 19 January 2023
Revised: 13 February 2023
Accepted: 13 February 2023
Published: 16 February 2023

1. Introduction

Currently, coal is a crucial energy source in today's society [1]; however, for a long time, the traditional combustion and utilization of coal has not only greatly reduced the quality of energy utilization but also caused serious environmental pollution problems (with the generation of SO_x, NO_x, greenhouse gases, etc.). Supercritical water gasification (SCWG) technology provides a promising method for the clean and efficient conversion of coal. It uses supercritical water as the reaction medium to convert hydrogen and carbon elements in the coal into H_2 and CO_2 [2–4].

Therefore, SCWG is considered to be a clean and efficient method for coal conversion that satisfies the need for both pollution prevention and the need for CO_2 reduction [5]. In past decades, various SCWG reactors, such as quartz tube reactors [6], tubular reactors [7] and fluidized bed reactors [8], have been designed to study various gasification mechanisms as well as product compositions.

Among these reactors, the supercritical water fluidized bed reactor (SCWFB) shows good performance [9] because it has the advantages of high heat and mass transfer rates, thus, achieving continuous and efficient gasification of high concentration coal slurry

and showing good prospects for commercial applications [10–12]. Matsumura and Minowa [8] first introduced a fluidized bed into the SCWG for wet biomass gasification.

Subsequently, Lv et al. [13] successfully established a SCWFB system for hydrogen production from biomass gasification using a model compound (glucose) and actual biomass (corn cobs) at 873 K in a continuous and stable manner, showcasing its clear advantages and good prospects. Jin et al. [14] improved the gasification efficiency of coal by using external recycling of liquid residuals. Due to the high temperature and pressure environment of SCWFB, it is difficult to obtain the detailed flow heat transfer characteristics by conventional experimental measurements. Thus, numerical simulation methods make up for the deficiencies of experimental studies and provide great convenience in understanding the flow and heat transfer characteristics in the reactor.

For instance, Su et al. [15] built a numerical simulation model of the gasification of biomass model compounds in the SCWFB, predicting the water–particle flow behavior, the temperature and reaction rate distribution and the gas composition distribution in the reactor. Ren et al. [16] then explored the radiation properties of supercritical water using the line-by-line (LBL) method and found that the thermal radiation plays an important role in the heat transfer of the reactor.

To well understand the SCWFB reactor, parameter analysis has been recently performed in the literature. In the parameters analysis of the SCWFB reactor, the wall temperature of the reactor is the most important parameter during the reaction process. It has been widely reported to affect the distribution of gas yield [10,17,18]. Therefore, the relationship between the desired gas production and the wall temperature of the reactor is important when designing and operating a SCWFB reactor. The effects of other parameters have also been investigated by, for example, changing the flow rate and the slurry concentration.

Li et al. [19] experimentally investigated the effects of the main operating parameters (the temperature, pressure, water flow rate, catalyst and coal slurry concentration) on the gasification in the SCWFB reactor. They found that a high temperature enhanced the hydrogen production, and the pressure had little significant effect on the gas production. Bei et al. [20] numerically investigated the effects of different operating parameters on the gasification products of ethanol, indicating that the wall temperature could significantly affect the carbon gasification rate and the gas yield.

Fan et al. [21] developed a numerical model of lignite gasification, which coupled the flow, the heat transfer and the gasification reaction. The temperature field, the particle residence time, the reaction rate and the product distribution in the reactor were investigated, and the bottleneck of complete gasification was revealed. However, for all the previously mentioned studies, the effects of the process parameters on the coal gasification were investigated independently. Due to the complex coupling effects among parameters, it is required to perform a comprehensive parameter analysis for better understanding of the performance of SCWFB reactor.

The coupled parameter analysis of the SCWFB reactor via numerical simulation, however, requires sampling a large number of points, the simulation of which is time consuming. To this end, this paper develops an efficient surrogate-assisted parametric analysis framework for the SCWFB reactor. Particularly, it first establishes a steady numerical simulation model of the SCWFB reactor for the subsequent analysis; and then it employs a Gaussian process (GP) surrogate modeling via efficient adaptive sampling to serve as an approximation for predicting the CE of the reactor (The GP has been recently used for the design, development and formulation of new products [22,23] since it performs well on the scenario with a few number of data points).

Based on this parameter analysis framework, this paper investigates the effects of the main parameters and their interactions on the reaction performance in terms of the CE, including the mass flow rate of supercritical water, the mass flow rate of the coal slurry, the temperature of supercritical water, the temperature of the outer wall and the reactor length.

The remainder of this paper is organized as follows. Section 2 first introduces the steady-state numerical model for the SCWFB reactor followed by the surrogate-based parametric modeling framework in Section 3. Thereafter, Section 4 comprehensively discusses the results and summarizes the main conclusions in Section 5.

2. Steady-State Numerical Model of the SCWFB Reactor

The three-dimensional geometry and operation conditions of the SCWFB reactor are shown in Figure 1a, where the coal slurry is injected into the reactor from the side and is mixed with the supercritical water injected from the bottom. The gasification of coal in supercritical water is an endothermic reaction in which the fluid mixture in the reactor is heated by two modes: (1) heated by four heating rods at a constant electric heating power and (2) heated by the isothermal outer wall of the reactor. Below, we provide the steady-state numerical model for the SCWFB reactor to describe the inner multi-phase flows as well as the reaction mechanism. This relatively fast numerical model would be used for data generation for the subsequent parameter analysis.

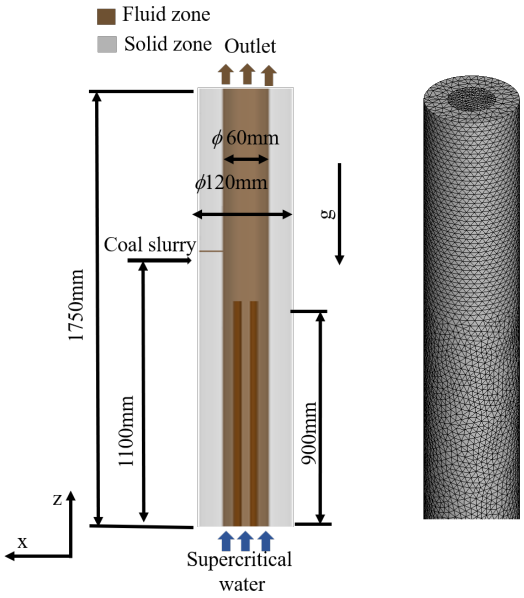

Figure 1. Illustration of (**a**) the SCWFB reactor as well as (**b**) the discrete numerical model.

2.1. Governing Equations

The physical model for the SCWFB reactor includes a continuous phase and discrete phase, and we use the subscripts f and p to represent them, respectively.

(1) Continuity equation:

$$\nabla \cdot (\rho_f \vec{v}_f) = S_m \tag{1}$$

where ρ_f and $\vec{v}_f$ are the density and velocity of fluid phase, and S_m denotes the mass transfer between two phases.

(2) Momentum conservation equation:

$$\nabla \cdot (\rho_f \vec{v}_f \vec{v}_f) = -\nabla p + \nabla \cdot \vec{\tau}_f + \rho_f \vec{g} - S_p \tag{2}$$

where $\vec{\tau}_f$ is the fluid viscous stress tensor, $\vec{g}$ is the mass force vector, and S_p is the momentum transferred from the discrete phase to the continuous phase.

(3) Energy conservation equation:

$$\nabla \cdot (\rho_f \vec{v}_f h_f) = \nabla \cdot (\lambda \nabla T - \sum_i h_i J_i) + q_{pf} + \vec{\tau}_f : \nabla \vec{v}_f + q_r \tag{3}$$

where $h_f = \sum_j Y_j h_j$, $h_i = h_i^0(T_{ref,i}) + \int_{Tref,j}^{T} c_{p,i} dT$, λ is the thermal conductivity of fluid, $h_i^0(T_{ref,i})$ is the standard mole enthalpy of the formation of species i, J_i is the diffusion flux of the i-th species, q_r is the radiation heat exchange source term, and finally q_{pf} represents energy transferred from the discrete phase to the continuous phase.

(4) Radiation equation:

Due to the high reactor temperature, the effect of radiative heat transfer is considered. The discrete ordinate (DO) radiation model is used to calculate the radiative heat transfer, and the DO equation can be expressed as

$$\frac{\mathrm{d}I(\vec{r},\vec{s})}{\mathrm{d}s} = k_f \frac{\sigma T_f^4}{\pi} + E_p - \left(k_f + k_p + \sigma_p\right) I(\vec{r},\vec{s}) + \frac{\sigma_p}{4\pi} \int_0^{4\pi} I\left(\vec{r},\vec{s}'\right) \Phi\left(\vec{s},\vec{s}'\right) d\Omega' \tag{4}$$

where E_p is the equivalent particle radiation, k_f and k_p are the radiation absorption coefficients of the fluid phase and discrete phase, respectively; σ_p is the particle scattering coefficient; and finally $d\Omega'$ represents the solid angle.

(5) Species transport equation:

$$\nabla \cdot \left(\rho_f Y_{f,i} \vec{v}_f\right) = \nabla \cdot \left(\rho_f D_{i,m} \nabla Y_{f,i}\right) + S_i \tag{5}$$

where $Y_{f,i}$ and $D_{i,m}$ are the mass fraction and diffusion coefficient of the i-th component in the fluid mixture, respectively; and S_i is the source term of the component resulting from the chemical reaction.

2.2. Reaction Mechanism

The gasification of coal in supercritical water is a complex conversion process involving both homogeneous and inhomogeneous reactions. It is accompanied by the formation of a large number of intermediates, and the gasification characteristics vary over the coal type and the reaction conditions. Su [24] developed a simplified kinetic model of coal supercritical water gasification reaction based on Guo's model [25]. The gasification process of coal in the SCWFB reactor is divided into the volatile pyrohydrolysis reactions, the fixed carbon reforming reaction, the water–gas shift reaction and the mathanation reaction. This model has the advantages of for example strong applicability to coal species. The chemical conversion of coal is described as follows.

(1) Volatile (Vol) pyrohydrolysis reaction:

$$\mathrm{Vol} \xrightarrow{k_1} \mathrm{H_2} \tag{6}$$

$$\mathrm{Vol} \xrightarrow{k_2} \mathrm{CO} \tag{7}$$

$$\mathrm{Vol} \xrightarrow{k_3} \mathrm{CH_4} \tag{8}$$

$$\mathrm{Vol} \xrightarrow{k_4} \mathrm{CO_2} \tag{9}$$

(2) Fixed carbon reforming reaction:

$$\mathrm{C} + \mathrm{H_2O} \xrightarrow{k_5} \mathrm{CO} + \mathrm{H_2} \tag{10}$$

$$\mathrm{C} + 2\mathrm{H_2O} \xrightarrow{k_6} \mathrm{CO_2} + 2\mathrm{H_2} \tag{11}$$

(3) Water gas shift reaction:

$$CO + H_2O \xrightarrow{k_7} CO_2 + H_2 \quad (12)$$

(4) Mathanation reaction:

$$CO + 3H_2O \xrightarrow{k_8} CO_2 + H_2 \quad (13)$$

It is worth noting that the mathanation reaction is not considered in the calculation due to the low reaction rate, and the rate constants at given temperatures and Arrhenius parameters of the above reactions can be found in Ref. [24].

2.3. Boundary Conditions and Numerical Scheme

In this paper, the Yimin lignite is used to conduct the simulation of coal gasification. The proximate and ultimate analysis of coal are given in Table 1. The IAPWS-IF97 [26] is used to calculate the physical parameters of supercritical water, and the radiation absorption coefficient of supercritical water is calculated by the line-by-line method (LBL) combined with the Planck weighted average [16].

The physical properties of the gasification products H_2, CO_2, CH_4 and CO are obtained from the NIST database [27], and the physical parameters of the mixed fluids are obtained by using the mass-weighted average of the corresponding physical properties of each component. The diffusion coefficients of each gas component in the supercritical water are obtained from the results of Zhao [28]. The coal particles are assumed to be spherical, and the specific physical parameters are shown in Table 2.

Table 1. Analysis of the Yimin coal.

Parameters	Yimin Coal (wt%)
Proximate analysis (air dried)	
Moisture	18.42
Fixed carbon	33.73
Volatile matter	32.21
Ash	15.46
Ultimate analysis (dry base)	
C	40.5
H	3.25
N	0.57
S	0.19
O	21.43

Table 2. Physical properties of the coal particles.

Parameters	Value
Density (kg/m^3)	1300
Specific heat ($J \cdot kg^{-1} \cdot K^{-1}$)	1680
Diameter (mm)	0.2264
Emissivity	0.9
Scattreing factor	0.6

It has been found that ignoring the heat conduction in the shell would overestimate the internal temperature of the reactor [16]. Hence, the coupled heat transfer process between the solid and fluid domains is considered in this modeling. The diameter of the inlet region of the slurry is very small in comparison to the length of the reactor.

In order to shorten the computational time, we used different cell sizes ranging from 1 to 10 mm and found that the final number of three-dimensional meshes of about 500,000 provides a good trade-off between accuracy and computational time (We refer to the results of

Bei et al. [20] that the number of mesh cells is 469,924 under the verification of mesh independence) as shown in Figure 1b. The near-wall y^+ value under this setting is about 100, which meets the requirement of the standard wall function (30< y^+<300) of the $k-\epsilon$ turbulence model [29].

The boundaries of the SCWFB reactor are as follows. The supercritical water and coal slurry are all set as mass-flow inlet, the reactor outlet is set as the pressure outlet, the outer wall of the reactor is the isothermal boundary condition, and the rest of walls adopt the adiabatic boundary condition. For the particle phase, all the walls are set as reflection boundary, indicating that the particles are bounced off once reaching the wall. In addition, all the particles could escape from the reactor outlet.

The ANSYS FLUENT 2022 R1 solver is used to solve the control equations of the SCWFB reactor. In this commercial computational fluid dynamics (CFD) solver, the first-order upwind method is used to discretize the convection term of the control Equations [21]; the Pressure-Implicit with Splitting of Operators (PISO) method is used to solve the pressure–velocity coupling problem [16]; the Renormalization Group (RNG) $k-\epsilon$ turbulence model is used for the continuous field solution [20]; and finally, the simulations are considered stable when the area-weighted average of the gas production at the reactor outlet remains constant.

2.4. Model Validation

The validation of the aforementioned SCWFB reactor simulation model is conducted by comparing the gas production near the outlet with the experimental results of Ren et al. [27]. Since the temperature is a key factor affecting the distribution of reaction products, two different temperature conditions are considered. The detailed operating conditions of the simulations are given in Table 3.

The simulation results and the experimental data of the outlet components of gas phase products are shown in Figure 2. The simulation results of all the gas productions agree well with the experimental results.The maximum deviation of gas production is 5.38 mol/kg per kg of coal, and the maximum percentage error of gas production is 6.31%. The main reason for the difference may be that the accuracy of the predicted values of CO_2 from the reaction equations decreases at a high temperature.

The mole fractions of gasification products of case 1 in the reaction process are shown in Figure 3. We found that the overall distribution and value range were similar to the high precision simulation results of Ren et al. [27]. The above analysis indicates that the reaction system of the SCWFB reactor model established in this paper is reasonable and will be adopted in the following experiments for data generation and analysis.

Table 3. Operating conditions for the SCWFB reactor.

Operating Conditions	Case 1	Case 2
Mass flow rate of the coal slurry (g/s)	0.3	0.3
Temperature of coal slurry (K)	298	298
Coal slurry concentration (wt%)	30	30
Mass flow rate of SCW (g/s)	2.7	2.7
Temperature of SCW (K)	773	823
Temperature of the outer wall temperature (K)	923	973
Total power of heating rods (W)	2000	2000

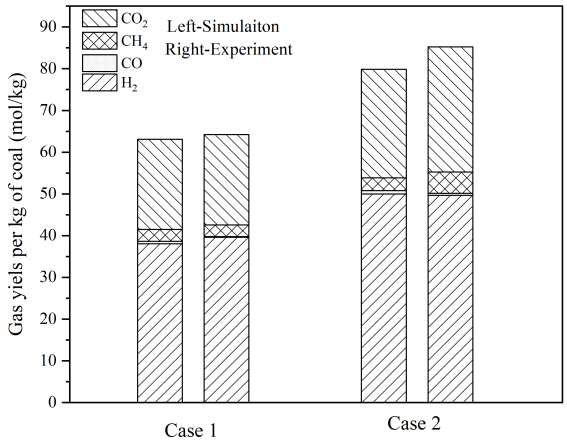

Figure 2. Comparison of the experimental and simulated gas productions.

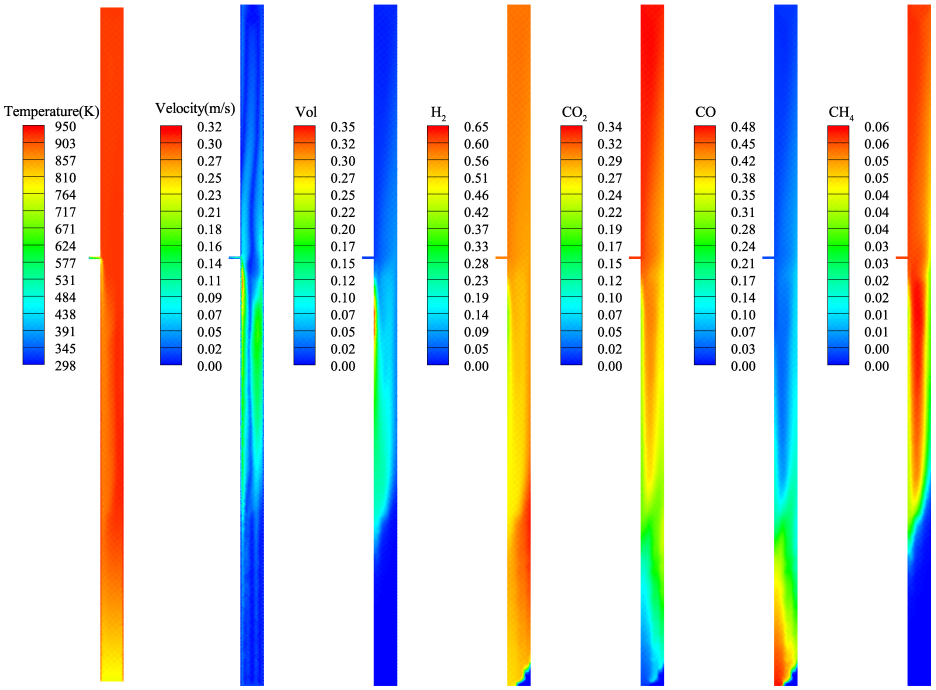

Figure 3. Cross-section plots of the temperature distribution, the velocity field and the mole fraction distributions of gasification products for the studied SCWFB reactor of Case 1.

3. Surrogate-Assisted Parametric Modeling Framework via Adaptive Sampling

An illustration of the GP based parametric modeling framework via adaptive sampling is presented in Figure 4. The method obtains data points from the boundary design space and simulates the CFD case automatically.

In the first step, we need to generate a series of initial sample points **X** and obtain their true response values **y** through the experimental design method and the previously built CFD model. Here, we adopt the well-known Latin hypercube sampling (LHS) [30] method. To further improve the quality of modeling, it needs sampling more points. The locations of the new sampled points will have a great impact on the prediction accuracy of the surrogate model.

One of the key issues in constructing a surrogate model is how to improve the accuracy through better selection of the new sample points. Here, we employ the effective CV-Voronoi adaptive sampling method [31], which sequentially query new points according to the information of surrogates. The key components, including the GP and the CV-Voronoi sampling method, will be elaborated in what follows.

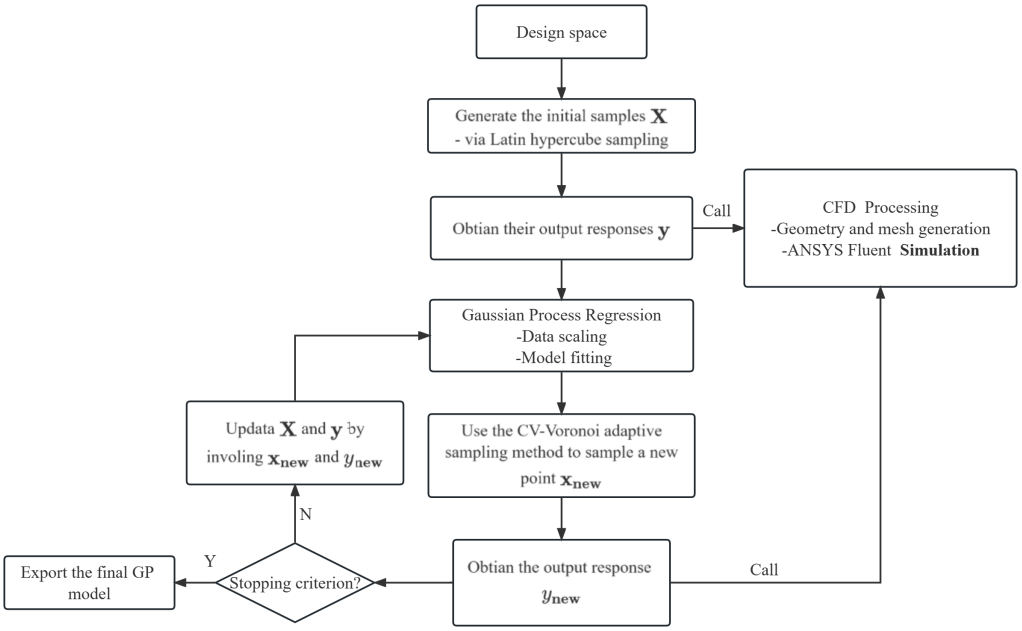

Figure 4. The flowchart of GP surrogating modeling via adaptive sampling.

3.1. Gaussian Process Regression

The Gaussian process (GP) is a data-driven Bayesian statistical method for modeling black-box functions. Compared to other surrogate models, such as linear regression and polynomial regression, it can learn nonlinear mappings and estimate uncertainty in the resulting predicted values. Therefore, the GP herein is used to approximate the relationships between various process parameters and the gas production.

The Gaussian process (GP) can be written as

$$f(\boldsymbol{x}_i) \sim GP(m(\boldsymbol{x}_i), k(\boldsymbol{x}_i, \boldsymbol{x}_j)) \tag{14}$$

where $m(\boldsymbol{x}_i)$ is the mean function, which is usually set to zero and without loss of generality [32]. The $k(\boldsymbol{x}_i, \boldsymbol{x}_j)$ is the covariance kernel function presenting the similarity between $\boldsymbol{x}_i$ and $\boldsymbol{x}_j$. Different kernel functions allow the model to capture different statistical features, such as the periodicity, invariance points and additivity. We chose the Matérn kernel, which is a generalization of the squared exponential kernel. The Matérn kernel function is defined as:

$$k(\boldsymbol{x}_i, \boldsymbol{x}_j) = \frac{1}{\Gamma(\nu)2^{\nu-1}} \left(\frac{\sqrt{2\nu}}{l} d(\boldsymbol{x}_i, \boldsymbol{x}_i) \right)^{\nu} J_{\nu} \left(\frac{\sqrt{2\nu}}{l} d(\boldsymbol{x}_i, \boldsymbol{x}_j) \right) \tag{15}$$

where ν is a positive parameter that controls the smoothness of the resulting function, and ν here is taken as $3/2$; $d(\cdot, \cdot)$ is the Euclidean distance; $J_{\nu}(\cdot)$ is a modified Bessel function; and finally, $\Gamma(\cdot)$ is the gamma function. It is more common to consider the effect of noise, $y_i = f(\boldsymbol{x}_i) + \epsilon_i$, where ϵ_i is an independently identically distributed Gaussian noise with variance σ_n^2.

The limited-memory Broyden–Fletcher–Goldfarb–Shanno (L-BFGS-B) optimization method was used to maximize the likelihood function, the optimized lengthscales in the kernel function are [0.9412, 0.8737, 0.4372, 1.0372, 1.2238], and the value of σ_n^2 is 0.102. When the hyperparameters have been optimized on the training data, the posterior predictive distribution of the GP model at test data $\boldsymbol{x}_*$ is given by a normal distribution, where the prediction mean and prediction variance can be expressed as follows:

$$\mu_*(\boldsymbol{x}_*) = \boldsymbol{K}_*(\boldsymbol{K} + \sigma_n^2 \boldsymbol{I})^{-1} y \tag{16}$$

$$\sigma_*^2(\boldsymbol{x}_*) = \boldsymbol{K}_{**} - \boldsymbol{K}_*(\boldsymbol{K} + \sigma_n^2\boldsymbol{I})^{-1}\boldsymbol{K}_*^T \tag{17}$$

where $\boldsymbol{K}_{(i,j)} = k(\boldsymbol{x}_i, \boldsymbol{x}_j)$ is the kernel matrix, $\boldsymbol{K}_{**} = k(\boldsymbol{x}_*, \boldsymbol{x}_*)$, $\boldsymbol{K}_* = [k(\boldsymbol{x}_*, \boldsymbol{x}_1), \cdots, k(\boldsymbol{x}_*, \boldsymbol{x}_n)]$, and $\boldsymbol{I}$ is the identity matrix.

3.2. Adaptive Sampling Strategies

Adaptive sampling, also known as active learning [33], sequentially determines the locations of sampling points through the information obtained from previous iterations. Currently, the adaptive sampling approaches can be divided into four categories [34], namely variance-based methods, query-by-committee-based methods, cross-validation-based methods and gradient-based methods. We choose a representative adaptive method, i.e., cross-validation (CV)-Voronoi, to generate the sample points for the modeling of the CE performance of the SCWFB reactor.

The CV-Voronoi method sequentially selects new points with the largest prediction error. It first partitions the entire design space into Voronoi tessellations, where a Voronoi cell corresponds to the region that is closer to a particular sample (the center point) than any other samples. Thereafter, the LOOCV (leave-one-out cross validation) technique is used to calculate the prediction error associated with each cell. The process is performed by: (1) removing a point from the sample set, (2) building a new surrogate model with the remaining points, (3) evaluating the new surrogate model at the removed point, and (4) calculating the LOO error, which can be expressed as:

$$e_{\mathrm{LOO}}^i = \left| f(\boldsymbol{x}_i) - \hat{\mu}_{*\boldsymbol{X}\setminus\boldsymbol{x}_i}(\boldsymbol{x}_i) \right| \tag{18}$$

where $f(\boldsymbol{x}_i)$ represents the real response at $\boldsymbol{x}_i$, $\hat{\mu}_{*\boldsymbol{X}\setminus\boldsymbol{x}_i}$ represents the predicted response at $\boldsymbol{x}_i$ by the surrogate model constructed on existing points without $\boldsymbol{x}_i$. Repeating this process for all cells and finding the Voronoi cell with the largest predicted error, the new sample point is then selected within the Voronoi cell with the largest error as well as the largest distance to the related center point $\boldsymbol{x}_c$. This is actually an optimization problem defined as:

$$\begin{aligned} \boldsymbol{x}_{new} &= \arg\max_{\boldsymbol{x}} d(\boldsymbol{x}, \boldsymbol{x}_c) \\ s.t.\ d(\boldsymbol{x}, \boldsymbol{x}_c) &- d_{min}(\boldsymbol{x}) = 0 \end{aligned} \tag{19}$$

where $d_{min}(\boldsymbol{x})$ is the minimal distance of $\boldsymbol{x}$ to existing points.

4. Results and Discussion

In this paper, five parameters, including the mass flow rate of supercritical water, mass flow rate of the coal slurry, temperature of supercritical water, temperature of the outer wall and reactor length, are selected as the input parameters. The base values of the five-parameters were chosen from Table 3, and the ranges of the five parameters refer to the results of Bei et al. [20] and Fan et al. [21].

The variable ranges of these variables and their symbols are presented in Table 4. Considering the primary functionality of the SCWFB reactor, the efficiency of converting the mass and energy content of the original feedstock into gaseous products is an important indicator. Hence, the carbon conversion efficiency, which is defined as the ratio of the total carbon in the gaseous products to the total carbon in the feedstock, is used to quantify the conversion of the SCWFB reactor. The CE criterion is expressed mathematically as:

$$CE(\%) = \frac{n_{CO_2} + n_{CO} + n_{CH_4}}{n_{c,feedstock}} \times 100 \tag{20}$$

where $n_{CO_2}, n_{CO}, n_{CH_4}$ and $n_{c,feedstock}$ represent the carbon moles in CO_2, CO, CH_4 and the feedstock, respectively.

Table 4. The values of selected variables of the SCWFB reactor.

Factor Name	Symbol	Range
Mass flow rate of SCW (g/s)	M_{SCW}	2∼4
Mass flow rate of the coal slurry (g/s)	M_C	0.3∼0.5
Temperature of the outer wall (K)	T_W	873∼973
Temperature of SCW (K)	T_{SCW}	723∼823
Reactor length (mm)	L	1500∼2000

4.1. The Validation of GP Model

The GP modeling start with five initial points. Then, the CV-Voronoi sampling method is employed to sequentially generate 40 informative points. That is, the stopping criterion in Figure 4 is the maximum number of points. The quality of the CV-Voronoi sampling results is evaluated on a separate test set by the root mean square error (RMSE), which can be written as:

$$RMSE = \sqrt{\frac{1}{M}\sum_{i=1}^{M}(\mu_*(\boldsymbol{x}_i) - y_i)^2} \tag{21}$$

where $M = 40$ is the size of the test set. Note that this test set is also sampling in the design space via LHS. Figure 5 shows the RMSE convergence curves of the CV-Voronoi method for the GP modeling of the CE of the SCWFB reactor. We found that the performance of the CV-Voronoi method is good, as the RMSE decreases fast and reaches stability after sampling 20 points.

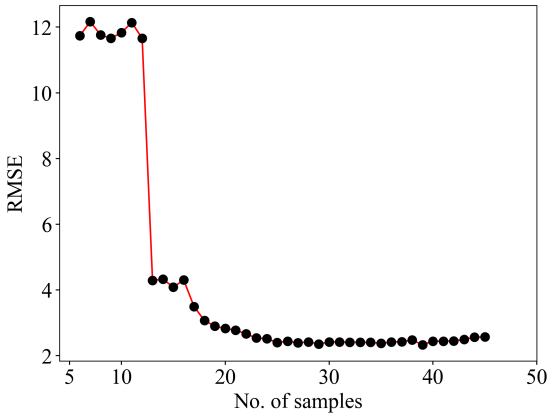

Figure 5. The RMSE convergence curve of the CV-Voronoi sampling process.

We further comprehensively evaluate the prediction quality of the developed GP model for the CE of the SCWFB reactor. The detailed performance of the GP model is reported in Table 5. The maximum and average deviations of the predicted CE are 10.89% and 3.16%, and the residual R^2 for the GP model is 0.95, indicating that the model describes the characteristics of the CE of the SCWFB reactor.

Table 5. Error analysis of the GP model.

Max Deviation (%)	Average (%)	RMSE	R^2
10.89	3.16	2.56	0.95

Figure 6 further illustrates the distribution of GP prediction, with the error bars indicating a 95% confidence interval. The diagonal dashed line represents the perfect agreement between the prediction and the simulated CE values. The diagonal dashed line runs through the confidence interval at most of the test points, indicating the excellent

accuracy of the prediction model. Therefore, the well-validated GP model will be used for the following parameter analysis of the SCWFB reactor.

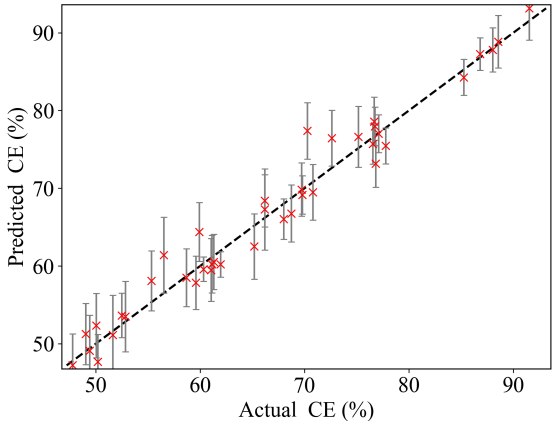

Figure 6. Diagonal plot of the GP predictions for the CE of the SCWFB reactor with the error bars indicating 95% confidence interval of the prediction.

4.2. Single-Parameter Analysis

Since the built GP model can provide fast yet accurate predictions over the whole domain, we can easily conduct single-parameter analysis of the CE and gas yield performance of the SCWFB reactor by varying one feature and keeping the other factors held constant.

Here, all the five parameters are to be investigated, keeping the remaining parameters in the middle of the parameter range. As we know, the GP model can obtain uncertainty in the resulting predicted values. In this section, the confidence interval is chosen to be 95%. First, the effect of mass flow rate of supercritical water on the CE and gas yield in the SCWFB reactor is shown in Figure 7a, and the CE and gas yield decreases slowly as the mass flow rate of supercritical water rises.

This is because the coal gasification in supercritical water is an endothermic reaction. Increasing the supercritical water flow rate will reduce the local temperature of the reactor, shorten the residence time of coal particles and inhibit the pyrohydrolysis reaction and the fixed carbon reforming reaction, thus, reducing the CE, H_2 and CO_2 of the reactor. The water gas shift reaction is also inhibited as the increase of supercritical water flow rate, thus, resulting in a gradual increase in CO.

Secondly, the effect of mass flow rate of the coal slurry on the CE and gas yield is investigated as shown in Figure 7b. With the increase of the coal slurry flow rate, the CE decreases slightly. In this paper, the coal slurry is considered to be composed of water and the corresponding carbon particles. Increasing the mass flow rate of the coal slurry will increase the flow rate of water and the heat absorption of the pyrohydrolysis reaction, both of which will reduce the temperature near the feed inlet of the reactor. This reduces the carbon conversion efficiency of reactor.

Although a higher mass flow rate of the coal slurry could increase the total gas products, the decrease in CE indicates a waste of raw material. However, if the coal slurry flow rate is too low, the heating potential of the supercritical water would not be fully utilized.

Thirdly, the effect of the outer wall temperatures on the coal gasification in supercritical water is investigated via the GP model. Figure 7c demonstrates the CE and gas-yield distribution within the SCWFB at different outer wall temperatures. It is apparent that the CE and H_2 increases significantly as the outer wall temperature rises. The relative increment of CE is about 100% when the outer wall temperature increases from 873 to 973 K.

This is because the high outer wall temperature will increase the overall temperature of the reactor and promotes the coal gasification reaction, which corresponds to the property

of endothermic reactions. Buhler et al. [35] indicated that the distribution of supercritical water gasification products is mainly affected by a free radical degradation at lower pressure and/or higher temperatures.

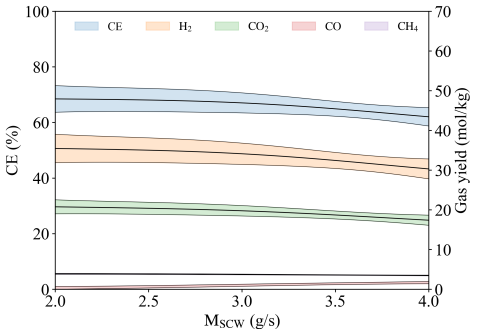

(**a**) Effect of the supercritical water flow rate

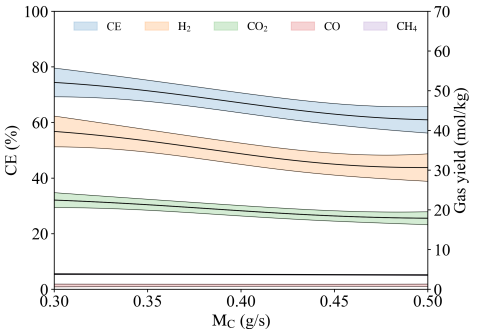

(**b**) Effect of the coal slurry flow rate

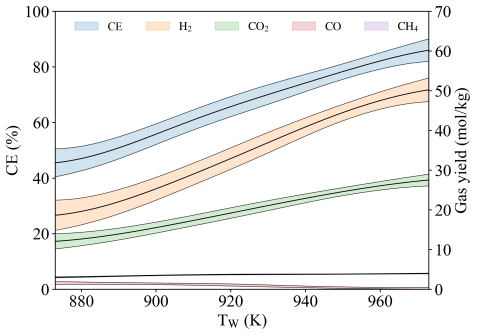

(**c**) Effect of the outer wall temperature

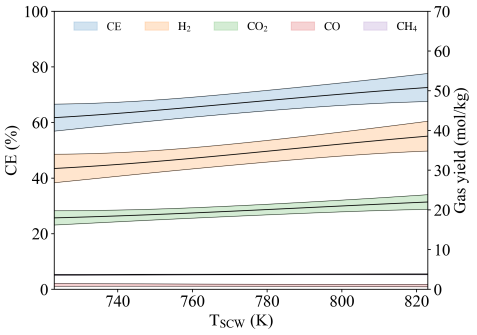

(**d**) Effect of the supercritical water temperature

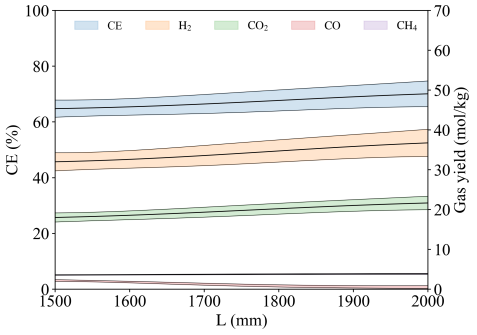

(**e**) Effect of the reactor length

Figure 7. Single-parameter analysis on the CE and the gas yield of the SCWFB reactor.

In addition, from the influence of the supercritical water temperature on the CE of reactor in Figure 7d, the CE increases smoothly as the supercritical water temperature increases gradually. As the supercritical water temperature rises, the inner temperature difference mainly occurs in the lower part of the reactor. Therefore, the rising supercritical water temperature will bring an increase in temperature near the inlet area of the reactor and then enhance the coal gasification reaction, eventually leading to an increase in CE.

Finally, Figure 7e shows that the CE and gas yield increase slowly with the increase of reactor length. This reveals that the CE and gas yield are insensitive to the reactor length. The reason is that the long reactor length will increase the particle residence time and then improve the coal gasification reaction. However, the four heating rods at the bottom of the reactor raise the surrounding temperature of the supercritical water. Consequently, the coal

gasification reaction mainly takes place at the bottom of the reactor, thus, weakening the effect of reactor length on the CE and the gas yield.

Table 6. Global sensitivity analysis of five parameters on the CE of the SCWFB reactor.

Factor Name	S_T	S_1	S_2
M_{SCW}	0.046	0.035	
M_C	0.066	0.055	
T_W	0.848	0.827	
T_{SCW}	0.058	0.051	
L	0.011	0.005	
M_{SCW}, T_W			0.006
M_C, T_W			0.006
L, T_W			0.004
M_C, T_{SCW}			0.002
T_W, T_{SCW}			0.002
M_{SCW}, T_{SCW}			0.001

4.3. Coupled Parameter Analysis

Through the previous analysis, we can qualitatively observe that the effect of the outer wall temperature on the reactor's CE is relatively large while the effect of the reactor length is small. To obtain a more complete picture of the effect of input parameters on the CE, we perform a global sensitivity analysis using the GP model to quantitatively obtain Sobol' total effects S_T, first-order S_1 and second-order S_2 [36].

Here, S_T measures the total contribution of the model inputs to the output variance, including the first-order component and the higher-order components. Differently, S_1 measures the contribution of individual input to the output variance, and S_2 measures the contribution of the interaction of two inputs to the output variance. Saltelli's method [37] was used to estimate the total and first Sobol' indices S_T, S_1 and S_2 with 4096 samples obtained from the GP model.

The results of the global parameter sensitivity analysis on the reactor's CE are presented in Table 6. The total sensitivity order for the CE is presented below: outer wall temperature > mass flow rate of the coal slurry > supercritical water temperature > mass flow rate of supercritical water > reactor length. The S_T value of the outer wall temperature in the global sensitivity is 0.848, which means it has more than 80% influence on the CE. Compared with other parameters, the outer wall temperature dominates the variation of CE and has a far greater influence. The value of S_1 is slightly smaller than S_T, which indicates that the contribution of the single parameter dominates the S_T. The results of S_2 are only given for values greater than 0.001. It can be seen that the largest S_2 is only 0.006, which indicates that the coupled effects of the parameters are almost negligible.

Furthermore, Figure 8 illustrates the two-dimensional contour plots of the CE performance with respect to any two features via the GP predictions. Here, all five parameters are investigated with the remaining parameters kept in the middle of the parameter range. The combined effect of the outer wall temperature and the supercritical water flow rate is shown in Figure 8b.

It can be observed that the CE increases with the increasing outer wall temperature and decreases with the increasing supercritical water flow rate, which is consistent with the previous analysis. In addition, the contour lines tend to be horizontal, indicating that the outer wall temperature is the dominant factor. The same behavior can be observed in Figure 8e,h,i. The slope of the contour lines in Figure 8c,j is close to 45°, which means that the effects of the coal slurry flow rate, supercritical water temperature and supercritical water flow rate on the CE are almost equivalent.

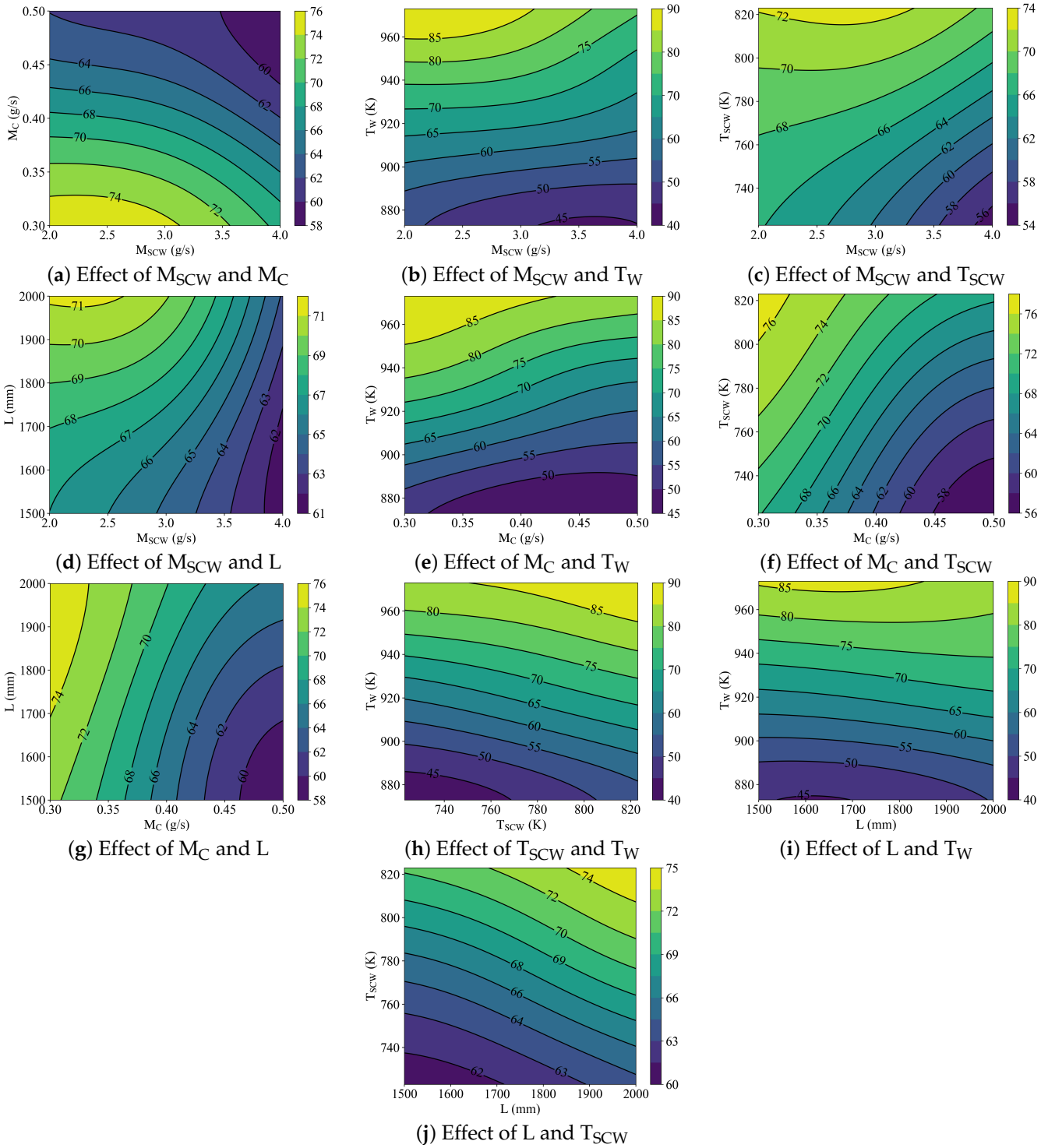

Figure 8. Two-dimensional contour plots of the coupled effect of parameters on the reactor's CE.

5. Conclusions

In this study, for performing efficient parametric analysis, a three-dimensional steady-state numerical model was developed to simulate the characteristics of a coal-SCWFB reactor. The numerical model was validated by experimental data. Thereafter, the GP was used to establish the surrogate model of the carbon conversion efficiency as a function of five parameters, including the mass flow rate of supercritical water, the mass flow rate of the coal slurry, the temperature of supercritical water, the temperature of the outer wall and the reactor

length based on the data generated by the CV-Voronoi adaptive sampling method and the numerical model. From the fast GP predictions, three conclusions are drawn below.

(1) A high R-squared value of 0.95 implies that the GP via CV-Voronoi sampling achieved good predictions with only a few points.
(2) The single-factor test of the gas yield and the CE showed that an increase in T_{SCW}, T_W and L enhanced the CE and the gas yield, while the increase of M_{SCW} and M_C inhibited them.
(3) The global sensitivity analysis results showed that T_W exerted a stronger effect than all the other factors on the CE. In addition, the coupled interaction between parameters had a slight effect on the CE, and the effect was mainly concentrated at the parameter boundaries of the design space.

Author Contributions: Conceptualization, P.Z. and H.L.; methodology, P.Z., H.L., R.X. and X.W.; software, P.Z., S.W. and J.L.; validation, P.Z. and S.W.; formal analysis, P.Z.; investigation, P.Z.; resources, P.Z., X.X. and S.Z.; data curation, P.Z.; writing—original draft preparation, P.Z.; writing—review and editing, P.Z.; visualization, P.Z.; supervision, H.L, R.X. and X.W.; project administration, X.W. and R.X.; and funding acquisition, X.W. and H.L. All authors have read and agreed to the published version of the manuscript.

Funding: This work was supported by the National Key Research and Development Program of China (2020YFA0714403), the National Natural Science Foundation of China (52005074) and the Natural Science Foundation of Liaoning Province (2022-MS-135).

Data Availability Statement: Not applicable.

Conflicts of Interest: The authors declare no conflict of interest.

Abbreviations

The following abbreviations are used in this manuscript:

SCWFB	Supercritical water fluidized bed
CE	Carbon conversion efficiency
SCWG	Supercritical water gasification
LBL	line-by-line
DO	discrete ordinate
GP	Gaussian process
CFD	Computational fluid dynamics
PISO	Pressure-implicit with splitting of operators
RNG	Renormalization group
LHS	Latin hypercude sampling
CV	Cross-validation
L-BFGS-B	Limited-memory Broyden–Fletcher–Goldfarb–Shanno
LOOCV	Leave-one-out cross validation

References

1. Schobert, H.H.; Song, C. Chemicals and materials from coal in the 21st century. *Fuel* **2002**, *81*, 15–32. [CrossRef]
2. Guo, L.; Jin, H. Boiling coal in water: Hydrogen production and power generation system with zero net CO_2 emission based on coal and supercritical water gasification. *Int. J. Hydrogen Energy* **2013**, *38*, 12953–12967. [CrossRef]
3. Hu, Y.; Gong, M.; Xing, X.; Wang, H.; Zeng, Y.; Xu, C.C. Supercritical water gasification of biomass model compounds: A review. *Renew. Sustain. Energy Rev.* **2020**, *118*, 109529. [CrossRef]
4. Lu, B.; Ge, Z.; Chen, Y.; Shi, J.; Jin, H. Study on supercritical water gasification reaction and kinetic of coal model compounds. *Fuel Process. Technol.* **2022**, *230*, 107210. [CrossRef]
5. Jin, H.; Fan, C.; Guo, L.; Zhao, X.; Cao, C.; Wei, W. Pore structure and its evolution in char during supercritical water gasification process. *J. Porous Media* **2019**, *11*, 159–207. [CrossRef]
6. Su, X.; Jin, H.; Guo, L.; Guo, S.; Ge, Z. Experimental study on Zhundong coal gasification in supercritical water with a quartz reactor: Reaction kinetics and pathway. *Int. J. Hydrogen Energy Process. Technol.* **2015**, *40*, 7424–7432. [CrossRef]
7. Bo, Y.; Wei, C.-h.; Hu, C.-s.; Cheng, X.; Wu, J.-z. Hydrogen generation from polyvinyl alcohol-contaminated wastewater by a process of supercritical water gasification. *J. Environ. Sci.* **2007**, *19*, 1424–1429.

8. Matsumura, Y.; Minowa, T. Fundamental design of a continuous biomass gasification process using a supercritical water fluidized bed. *Int. J. Hydrogen Energy* **2004**, *29*, 701–707. [CrossRef]
9. Zhang, T.; Lu, Y. Modeling of Wall-to-Bed Heat Transfer in a Supercritical Water Fluidized Bed by the Packet Approach. *Ind. Eng. Chem. Res.* **2020**, *59*, 22640–22655. [CrossRef]
10. Jin, H.; Lu, Y.; Liao, B.; Guo, L.; Zhang, X. Hydrogen production by coal gasification in supercritical water with a fluidized bed reactor. *Int. J. Hydrogen Energy* **2010**, *35*, 7151–7160. [CrossRef]
11. Goodwin, A.K.; Rorrer, G.L. Reaction rates for supercritical water gasification of xylose in a micro-tubular reactor. *Chem. Eng. J.* **2010**, *163*, 10–21. [CrossRef]
12. Huang, J.; Lu, Y.; Jia, L. Experimental study on the two-phase flow structure in a supercritical water-fluidized bed. *Ind. Eng. Chem. Res.* **2019**, *58*, 20099–20108. [CrossRef]
13. Lu, Y.J.; Jin, H.; Guo, L.J.; Zhang, X.M.; Cao, C.Q.; Guo, X. Hydrogen production by biomass gasification in supercritical water with a fluidized bed reactor. *Int. J. Hydrogen Energy* **2008**, *33*, 6066–6075. [CrossRef]
14. Jin, H.; Fan, C.; Guo, L.; Liu, S.; Cao, C.; Wang, R. Experimental study on hydrogen production by lignite gasification in supercritical water fluidized bed reactor using external recycle of liquid residual. *Energy Convers. Manag.* **2017**, *145*, 214–219. [CrossRef]
15. Su, X.; Jin, H.; Guo, S.; Guo, L. Numerical study on biomass model compound gasification in a supercritical water fluidized bed reactor. *Chem. Eng. Sci.* **2015**, *134*, 737–745. [CrossRef]
16. Ren, Z.; Guo, L.; Jin, H.; Luo, K. Integration of CFD codes and radiation model for supercritical water gasification of coal in fluidized bed reactor. In Proceedings of the International Heat Transfer Conference, Beijing, China, 10–15 August 2018; Digital Library, Begel House Inc.: Danbury, CT, USA, 2018.
17. Jin, H.; Chen, Y.; Ge, Z.; Liu, S.; Ren, C.; Guo, L. Hydrogen production by Zhundong coal gasification in supercritical water. *Int. J. Hydrogen Energy* **2015**, *40*, 16096–16103. [CrossRef]
18. Yao, L.; Lu, Y. Supercritical water gasification of glucose in fluidized bed reactor: A numerical study. *Int. J. Hydrogen Energy* **2017**, *42*, 7857–7865. [CrossRef]
19. Li, Y.; Guo, L.; Zhang, X.; Jin, H.; Lu, Y. Hydrogen production from coal gasification in supercritical water with a continuous flowing system. *Int. J. Hydrogen Energy* **2010**, *35*, 3036–3045. [CrossRef]
20. Bei, L.; Ge, Z.; Ren, C.; Su, D.; Ren, Z.; Guo, L. Numerical study on supercritical water partial oxidation of ethanol in a continuous reactor. *Energy* **2022**, *249*, 123750. [CrossRef]
21. Fan, C.; Guo, S.; Jin, H. Numerical study on coal gasification in supercritical water fluidized bed and exploration of complete gasification under mild temperature conditions. *Chem. Eng. Sci.* **2019**, *206*, 134–145. [CrossRef]
22. Ringstad, K.E.; Banasiak, K.; Ervik, Å.; Hafner, A. Machine learning and CFD for mapping and optimization of CO_2 ejectors. *Appl. Therm. Eng.* **2021**, *199*, 117604. [CrossRef]
23. Bahrainian, S.S.; Bakhshesh, M.; Hajidavalloo, E.; Parsi, M. A novel approach for solid particle erosion prediction based on Gaussian Process Regression. *Wear* **2021**, *466*, 203549. [CrossRef]
24. Su, X.; Guo, L.; Jin, H. Mathematical modeling for coal gasification kinetics in supercritical water. *Energy Fuels* **2016**, *30*, 9028–9035. [CrossRef]
25. Guo, S.; Guo, L.; Yin, J.; Jin, H. Supercritical water gasification of glycerol: Intermediates and kinetics. *J. Supercrit. Fluids* **2013**, *78*, 95–102. [CrossRef]
26. Wagner, W.; Kretzschmar, H.-J. IAPWS industrial formulation 1997 for the thermodynamic properties of water and steam. In *International Steam Tables: Properties of Water and Steam Based on the Industrial Formulation IAPWS-IF97*; Springer: Berlin/Heidelberg, Germany, 2008; pp. 7–150.
27. Ren, J.; Liu, Z.; Changsheng, L. Numerical Analysis of Particle Flow and Heat Transfer Characteristics in a Coal-Supercritical Water Fluidized Bed Reactor for Hydrogen Production. *J. Eng. Thermophys.* **2020**, *41*, 154–160.
28. Zhao, X.; Jin, H.; Chen, Y.; Ge, Z. Numerical study of H_2, CH_4, CO, O_2 and CO_2 diffusion in water near the critical point with molecular dynamics simulation. *Comput. Math. Appl.* **2021**, *81*, 759–771. [CrossRef]
29. Saiful Alam, M.; Wijayanta, A.T.; Nakaso, K.; Fukai, J. Study on coal gasification with soot formation in two-stage entrained-flow gasifier. *Int. J. Energy Environ. Eng.* **2015**, *6*, 255–265. [CrossRef]
30. McKay, M.D.; Beckman, R.J.; Conover, W.J. A comparison of three methods for selecting values of input variables in the analysis of output from a computer code. *Technometrics* **2020**, *42*, 55–61. [CrossRef]
31. Xu, S.; Liu, H.; Wang, X.; Jiang, X. A robust error-pursuing sequential sampling approach for global metamodeling based on voronoi diagram and cross validation. *J. Mech. Des.* **2014**, *136*, 071009. [CrossRef]
32. Alamaniotis, M.; Chatzidakis, S.; Tsoukalas, L.H. Monthly load forecasting using kernel based Gaussian process regression. In Proceedings of the ninth Mediterranean Conference on Power Generation, Transmission, Distribution and Energy Conversion: MEDPOWER 2014, Athens, Greeece, 2–5 November 2014.
33. Settles, B. *Active Learning Literature Survey*; Computer Science Technical Report; University of Wisconsin-Madison: Madison, WI, USA, 2009; p. 1684.
34. Liu, H.; Ong, Y.-S.; Cai, J. A survey of adaptive sampling for global metamodeling in support of simulation-based complex engineering design. *Struct. Multidiscip. Optim.* **2018**, *57*, 393–416. [CrossRef]

35. Bühler, W.; Dinjus, E.; Ederer, H.J.; Kruse, A.; Mas, C. Ionic reactions and pyrolysis of glycerol as competing reaction pathways in near-and supercritical water. *J. Supercrit. Fluids* **2002**, *22*, 37–53.[CrossRef]
36. Kucherenko, S.S.; Sobol', I.M. Global sensitivity indices for nonlinear mathematical models, Review. *Wilmott* **2005**, *1*, 56–61.
37. Saltelli, A.; Annoni, P.; Azzini, I.; Campolongo, F.; Ratto, M.; Tarantola, S. Variance based sensitivity analysis of model output. Design and estimator for the total sensitivity index. *Comput. Phys. Commun.* **2010**, *181*, 259–270. [CrossRef]